



## Fabrication of Anastomosed Tubular Networks Developed out of Fenestrated Sheets through Thermo Responsiveness of Polymer Giant Vesicles

Eri Yoshida\*

Department of Environmental and Life Sciences, Toyohashi University of Technology, Japan

\*Corresponding author: Eri Yoshida, Department of Environmental and Life Sciences, Toyohashi University of Technology, Toyohashi, Japan, Tel: +81532446814; E-mail: eyoshida@ens.tut.ac.jp

Received: February 15, 2017; Accepted: February 21, 2017; Published: February 24, 2017

### Abstract

The thermo responsive behavior of spherical vesicles and worm-like vesicles composed of amphiphilic poly(methacrylic acid)-*block*-poly(methyl methacrylate-*random*-methacrylic acid) diblock copolymer, PMAA-*b*-P(MMA-*r*-MAA), was investigated in order to elucidate their morphological transformation and thermal stability. The spherical vesicles comprised of PMAA<sub>195</sub>-*b*-P(MMA<sub>0.817</sub>-*r*-MAA<sub>0.183</sub>)<sub>224</sub> were disrupted into smaller spherical vesicles by an increase in temperature, followed by much smaller micelles, and finally into planar aggregates consisting of the micelles. A decrease in the temperature produced spherical vesicles smaller than the original ones. A rapid temperature decrease of the planar aggregates, followed by the ripening simultaneously provided anastomosed tubular networks and fenestrated sheets as seen in some organelles. The tubular networks consisted of round swollen tubules and were continuous with the fenestrated sheets. The worm-like vesicles of PMAA<sub>351</sub>-*b*-P(MMA<sub>0.826</sub>-*r*-MAA<sub>0.174</sub>)<sub>372</sub> were transformed into shorter and spherical vesicles and finally into fused aggregates by the temperature increase. By decreasing the temperature, the worm-like vesicles were reproduced from the fused aggregates through the formations of partial sheets and branched tubules, however, they were round and shorter than the original vesicles. It was found that the worm-like vesicles were more thermally stable than the spherical vesicles at the same vesicle concentration and retained the vesicle structure even at the high temperature.

**Keywords:** Thermo responsiveness; Spherical vesicles; Worm-like vesicles; Anastomosed tubular networks; Fenestrated sheets

### Introduction

Lipid bilayer membrane composing biomembranes continually undergoes budding and fusion in living cells to maintain its living activity. Endocytosis initiated by budding from plasma membrane takes foreign substances, such as bacteria, into a cell to digest them [1,2]. Oppositely, exocytosis achieved by fusion of lipid bilayer vesicles to plasma membrane releases neurotransmitters and hormones delivered by the vesicles into the outside of the cell [3]. The membrane budding and fusion play especially important roles in the vesicular transport between organelles. Proteins synthesized by rough endoplasmic reticulum are carried to Golgi apparatus through sequential processes of the budding of vesicles from the rough endoplasmic reticulum, transport by the vesicles, and finally membrane fusion of the vesicles to the Golgi apparatus [4]. The transport of substances including the proteins between the Golgi stacks is also based on the continuous budding and fusion of Golgi vesicles [5,6]. Hence, these organelles have heterogeneous structures corresponding to the budding and fusion [7,8]; the cis region of the Golgi facing the endoplasmic reticulum and receiving the transport vesicles from it is a sheet with many fenestrations, while the trans region providing vesicles by the budding to deliver the substances to the plasma membrane and other organelles of lysosome consists of anastomosed tubular networks [9,10]. The

**Citation:** Yoshida E. Fabrication of Anastomosed Tubular Networks Developed out of Fenestrated Sheets through Thermo responsiveness of Polymer Giant Vesicles. ChemXpress 2017;10(1):118.

© 2016 Trade Science Inc

Golgi cisternae are partitioned into numerous vesicles during cell division and are reconstructed from these vesicles during the telophase [11-14].

Giant vesicles consisting of amphiphilic poly(methacrylic acid)-*block*-poly(methyl methacrylate-*random*-methacrylic acid) diblock copolymer, PMAA-*b*-P(MMA-*r*-MAA), are possible artificial biomembrane models of cells and organelles based on the similarities in their structure and responsiveness [15-18]. The similarities also include the morphological variation of the vesicles based on critical packing shape [19] of the diblock copolymer. The vesicles varied the morphology from spherical to elliptical [20], worm-like [21], villus-like [22], key-shaped [23], and sheet [24-26], depending on the block length, hydrophilic-hydrophobic balance, mixed composition, and solvent quality for the vesicle preparation [20-28]. It has been reported that the vesicles underwent budding and fusion in response to variations in the circumstances, such as temperature [15] and pH [29]. In this study, fenestrated sheets as seen in the cis region of the Golgi apparatus and anastomosed tubular networks in the trans region were fabricated through thermoresponsiveness of the polymer giant vesicles. This paper describes the thermoresponsive behavior of the giant vesicles comprised of PMAA-*b*-P(MMA-*r*-MAA) and the fabrication of fenestrated sheets and anastomosed tubular networks through their thermo responsiveness.

## Experimental

### Instrumentation

Light scattering measurements were performed with a Photal Otsuka Electronics ELS-8000 electrophoretic light scattering spectrophotometer equipped with a system controller, an ELS controller, and a He-Ne laser operating  $\lambda=632.8$  nm. The transmittance of a vesicle solution was obtained using a Shimadzu UV-160A UV-Vis recording spectrophotometer. Field emission scanning electron microscopy (FE-SEM) measurements were performed using a Hitachi SU8000 scanning electron microscope.

### Materials

The spherical vesicles [15] and worm-like vesicles [23] were prepared by the photo polymerization-induced self-assembly are using the nitroxide-mediated photo-controlled/living radical polymerization technique [30]. The spherical vesicles were comprised of PMAA<sub>195</sub>-*b*-P(MMA<sub>0.817</sub>-*r*-MAA<sub>0.183</sub>)<sub>224</sub> (Mn=36,600 and Mw/Mn=1.52 by gel permeation chromatography based on PMAA standards), while the worm-like vesicles were composed of PMAA<sub>351</sub>-*b*-P(MMA<sub>0.826</sub>-*r*-MAA<sub>0.174</sub>)<sub>372</sub> (Mn=100,500 and Mw/Mn=1.68). Methanol (MeOH) was refluxed over magnesium with a small amount of iodine and distilled.

### Light scattering measurement

The spherical vesicles (108 mg) were dispersed in an aqueous methanol solution (MeOH/water=3/1 v/v, 4 mL) by vigorous shaking, then subjected to light scattering measurements. Similarly, the worm-like vesicles (27 mg) in an aqueous methanol solution (4 mL) were used for light scattering measurements. The light scattering measurements were performed at the angle  $\theta=90^\circ$  at designated temperatures. The hydrodynamic size (Dh) of a vesicle diameter was estimated by the cumulant analysis, while the scattering intensity distribution was obtained by the Marquardt analysis [31].

SEM observations.

The vesicles in an aqueous methanol solution were dried in air and subjected to FE-SEM measurements. The morphologies and vesicular size were determined by the FE-SEM observation at 1.0 kV without coating. The size distribution of vesicles was estimated as reported previously [32].

## Results and Discussion

The thermo responsiveness of the giant vesicles comprised of PMAA-*b*-P(MMA-*r*-MAA) was investigated in an aqueous methanol solution (MeOH/water=3/1 v/v). The investigation was performed for the spherical vesicles and worm-like vesicles. The spherical

vesicles consisting of  $\text{PMAA}_{195}\text{-}b\text{-P(MMA}_{0.817}\text{-}r\text{-MAA}_{0.183})_{224}$  had a  $4.74\ \mu\text{m}$  diameter ( $D_n$ ) and 1.31 of size distribution ( $D_w/D_n$ ) [15], while the worm-like vesicles of  $\text{PMAA}_{351}\text{-}b\text{-P(MMA}_{0.826}\text{-}r\text{-MAA}_{0.174})_{372}$  had  $D_n(L)=3.41\ \mu\text{m}$  and  $D_w/D_n(L)=1.56$  for the long axis and  $D_n(S)=0.437\ \mu\text{m}$  and  $D_w/D_n(S)=1.06$  for the short axis, respectively [23]. FIG. 1 shows the variation in light scattering intensity of the spherical vesicles and their hydrodynamic size ( $D_h$ ) of the diameter versus temperature. A good hysteresis was obtained for the scattering intensity, whereas the vesicle size showed a poor hysteresis for the temperature changes. The hydrodynamic size rapidly decreased to ca.  $0.3\ \mu\text{m}$  over  $30^\circ\text{C}$  and slightly increased at  $50^\circ\text{C}$ , suggesting the disruption of the vesicles into smaller particles by the temperature increase and the aggregation of the particles by the further increase in the temperature. The FE-SEM demonstrated that the formation and aggregation of small particles produced by the disruption due to the temperature increase. FIG. 2 shows the SEM images and scattering intensity distributions of the spherical vesicles for each temperature. Part of the SEM images has been previously reported [15], however, the SEM analysis in the present study focused on the variation in particle size. The scattering intensity distribution continued to shift to a lower side of the hydrodynamic size up to  $45^\circ\text{C}$  and was shifted to its higher side at  $50^\circ\text{C}$  throughout a wide range of even over  $10\ \mu\text{m}$ . The vesicles were partitioned into smaller spherical vesicles by the temperature increase, and further into planar aggregates. It was found that this transformation from the spherical vesicles into planar aggregates was caused by the opening of the spherical vesicles due to the expansion of a hole on the vesicle surface based on the observation of bowl-like vesicles. A detailed analysis revealed that the planar aggregates consisted of much smaller micelles produced by further disruption of the small spherical vesicles (FIG. 2e). The micelles had a  $0.408\ \mu\text{m}$  diameter and 1.17 in size distribution. It was expected that water molecules hydrating to the MAA units in the hydrophobic  $\text{P(MMA-}r\text{-MAA)}$  blocks were excluded from the hydrophobic area due to the temperature increase, causing a change in critical packing shape of the diblock copolymer from a truncated cone that formed spherical vesicles to a cone to produce micelles (SCHEME. 1). By decreasing the temperature from  $50^\circ\text{C}$  to  $35^\circ\text{C}$ , spherical vesicles were reproduced by separation from the planar aggregates (FIG. 3). However, a further decrease in the temperature yielded spherical vesicles smaller than the original vesicles by the disruption of the reproduced vesicles. The size of the resulting vesicles was  $D_n=1.01\ \mu\text{m}$  and  $D_w/D_n=1.12$ .

It was found that a rapid temperature decrease of the planar aggregate solution from  $50^\circ\text{C}$  to  $25^\circ\text{C}$  provided different morphology. FIG. 4 shows the FE-SEM images of the morphology formed by the rapid temperature decrease operation. Incomplete and partially fused spherical vesicles were produced just after the temperature decrease. These were transformed into sheets with many fenestrations and anastomosed tubular networks as seen in the Golgi apparatus and endoplasmic reticulum [7-10], by the ripening in an aqueous MeOH solution at room temperature for 8 days. The sheets had fenestrations with a  $0.186\ \mu\text{m}$  diameter on average, while the networks consisted of round swollen tubules with  $1.61\ \mu\text{m}$  in thickness. It is expected that spherical vesicles were produced by

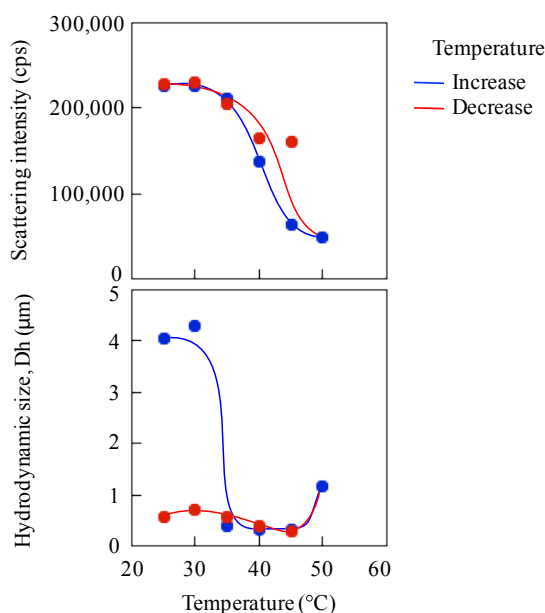
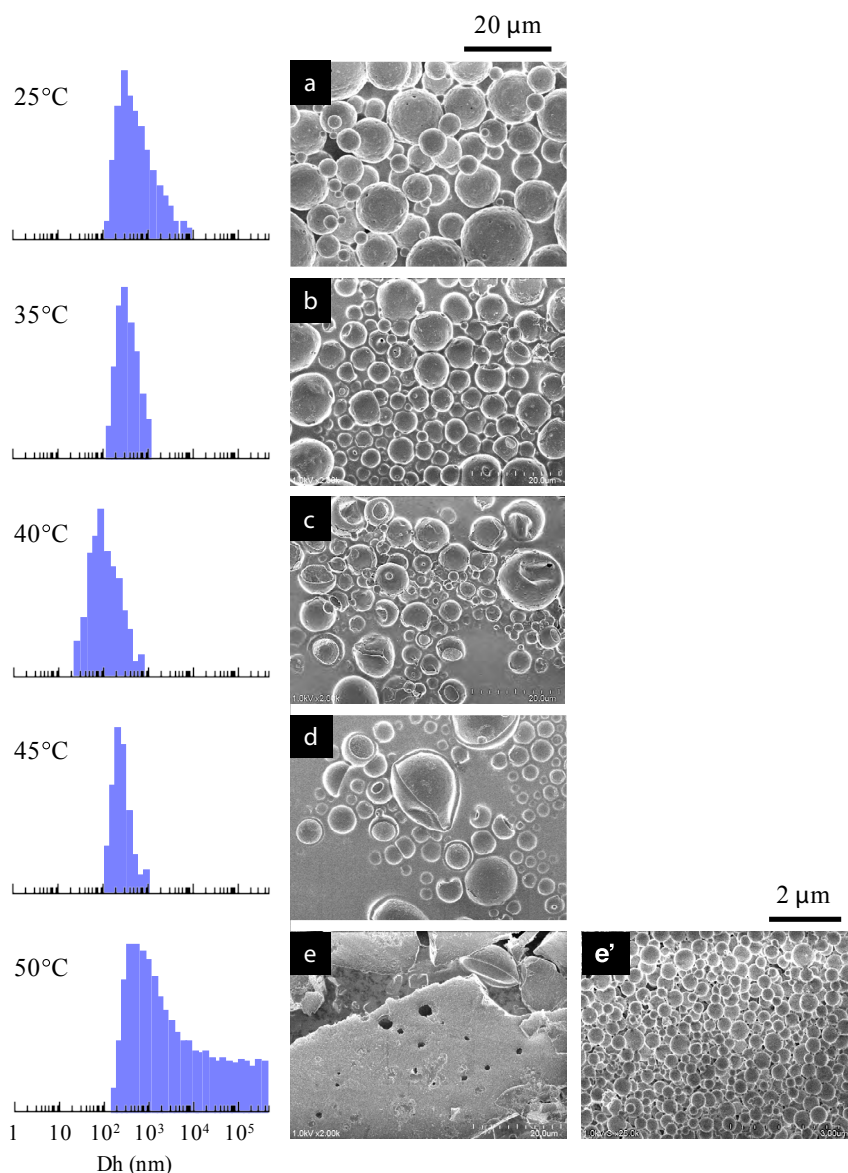


FIG. 1. The light scattering intensity and hydrodynamic size ( $D_h$ ) of the spherical vesicles versus the temperature. The vesicle concentration= $27.0\ \text{g/L}$ .

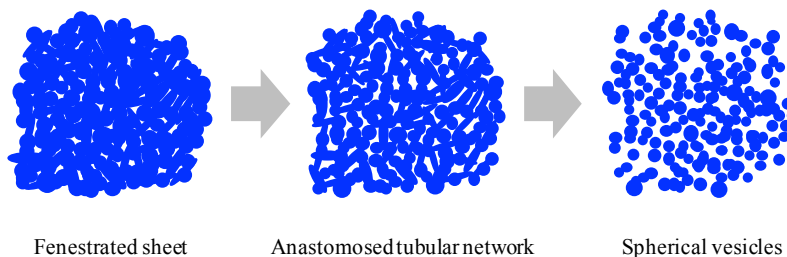


**FIG. 2. The SEM images and scattering intensity distributions of the spherical vesicles for the temperature increase: a 25°C, b 35°C, c 40°C, d 45°C, e 50°C, and e' the high magnification for 50°C. The vesicle concentration=27.0 g/L.**

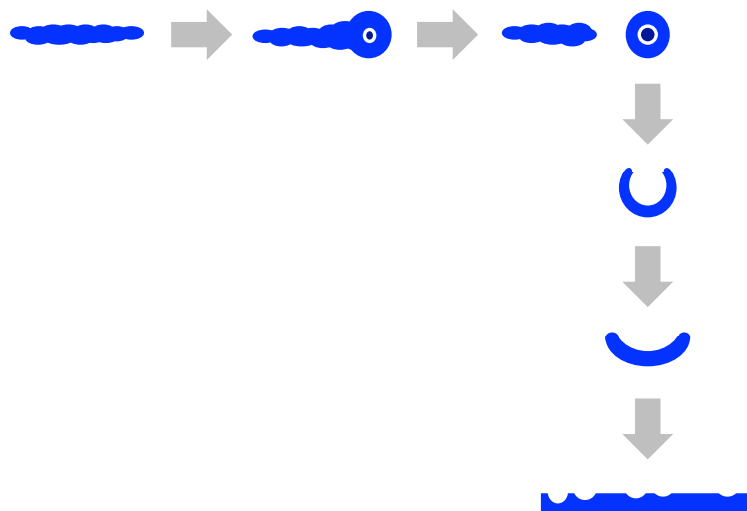
the budding separation from these tubules. Furthermore, the anastomosed tubular network was continuous with the fenestrated sheet (FIG. 4d), indicating that the tubular networks were formed by expansion of the fenestrations on the sheets (SCHEME. 2).

The worm-like vesicles showed different thermo responsiveness from the spherical vesicles in the light scattering study. They produced a slight change in the scattering intensity throughout the variation in the temperature and showed a good hysteresis (FIG. 5). The vesicles also showed a good hysteresis for the hydrodynamic size versus the temperature changes. However, the hydrodynamic size of the worm-like vesicles was averaged for their long and short axes. Accordingly, the transmittance of the worm-like vesicle solution was employed for the investigation of the thermo responsiveness. The transmittance based on the UV absorbance at 250 nm continued to increase with the temperature increase, suggesting the formation of much smaller particles by the disruption of the worm-like vesicles. The transmittance showed negligible changes by decreasing the temperature and did not revert to the original value. The FE-SEM analysis demonstrated that the worm-like vesicles were transformed into various short worm-like and spherical vesicles due to the temperature increase. As shown in FIG. 6, the initial thin and rough-edged worm-like vesicles at 25°C were partially swollen at the middle and end by the temperature increase and were transformed into fused aggregates by its further increase. Many holes were observed on the surface of the aggregates by the opening of the vesicles, implying that





**SCHEME. 2. The variation in the morphology from the fenestrated sheet into anastomosed tubular network and finally into spherical vesicles.**



**SCHEME. 3. The morphology changes from the worm-like vesicles into the fused planar aggregates by the temperature increase through the expansion of the worm-like vesicles, separation of spherical vesicles from the worm-like vesicles, and the opening of holes on the spherical vesicles.**

the expansion of hollows inside of the worm-like vesicles was a trigger to vary the vesicle morphology (SCHEME. 3). As the temperature decreased, worm-like vesicles were reproduced from the fused aggregate matrix through the transformation into partial sheets, followed by the anastomosed tubules (FIG. 7). However, the reproduced worm-like vesicles were rounded, smooth-edged, and short ( $D_n(L)=2.02 \mu\text{m}$ ,  $D_w/D_n(L)=1.44$  and  $D_n(S)=0.692 \mu\text{m}$ ,  $D_w/D_n(S)=1.16$ ) as compared with the original vesicles. The resulting vesicles were still shortened by the ripening in an aqueous MeOH solution for 7 days at room temperature ( $D_n(L)=1.47 \mu\text{m}$ ,  $D_w/D_n(L)=1.62$ ), although there was a negligible change in thickness ( $D_n(S)=0.680 \mu\text{m}$ ,  $D_w/D_n(S)=1.21$ ). It is considered that the diblock copolymers were rearranged in a more thermally stable state within the vesicles to reduce the hydrophobic volume at the high temperature and during the ripening, resulting in the formation of the short worm-like vesicles with the smooth surfaces. In addition, the worm-like vesicles caused no fusion at  $50^\circ\text{C}$  for a higher vesicle concentration, the same as the concentration for the study on the thermo responsiveness of the spherical vesicles (FIG. 8). The worm-like vesicles had the vesicle structure even at  $50^\circ\text{C}$  without fusion, accompanied by the morphological change into the rounded and spherical vesicles. It was found that the worm-like vesicles were more thermally stable than the spherical vesicles and retained their vesicular structure at the high temperature. This thermal stability of the worm-like vesicles may be one of the reasons that many organelles and bacteria take worm-like and tubular shapes, while transport vesicles are spherical.

## Conclusions

The spherical vesicles were disrupted into smaller vesicles by an increase in the temperature, followed by into much smaller micelles, and finally into planar aggregates consisting of the micelles. A decrease in the temperature reproduced vesicles smaller than the original vesicles. A rapid decrease in the temperature of the planar aggregates, followed by their ripening simultaneously

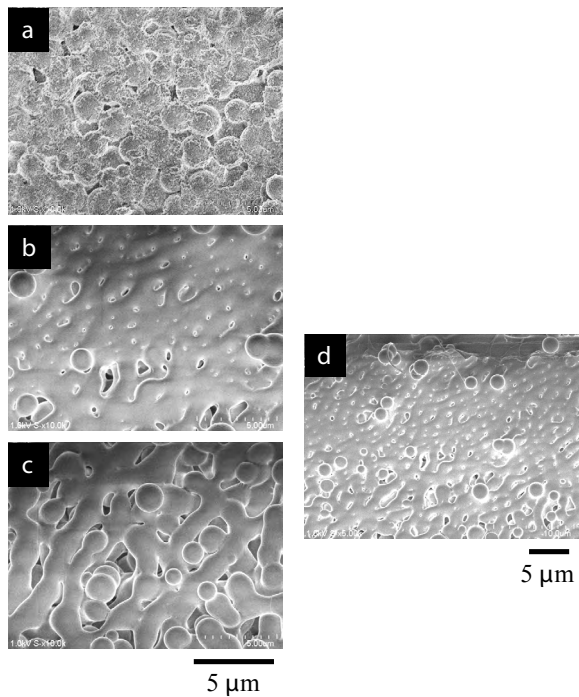


FIG. 4. The FE-SEM images of the morphology obtained by the rapid temperature decrease and the ripening in an aqueous MeOH solution at room temperature for 8 days: a without the ripening, b a fenestrated sheet, c an anastomosed tubular network, and d the tubular network continuous with the sheet. The vesicle concentration = 27.0 g/L.

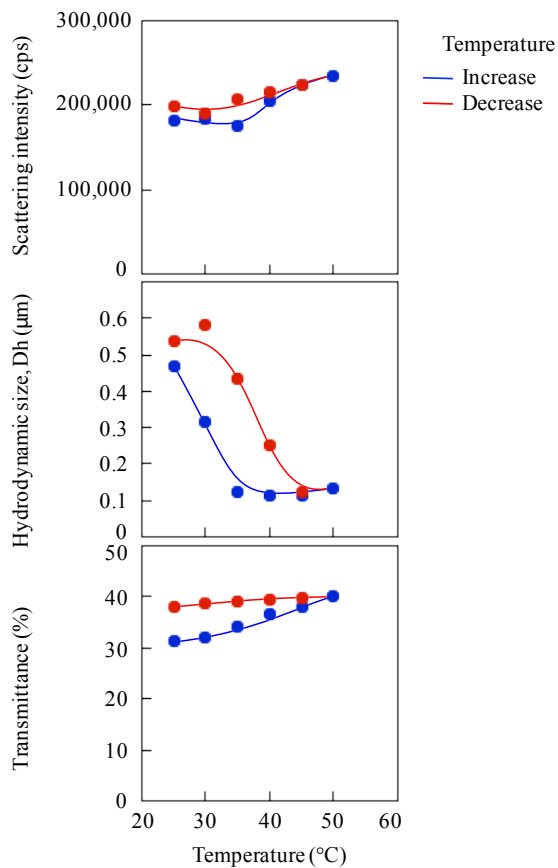
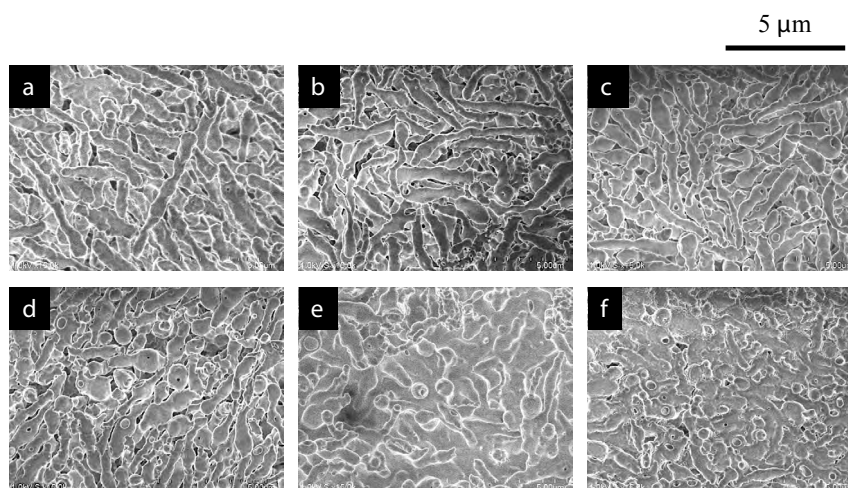
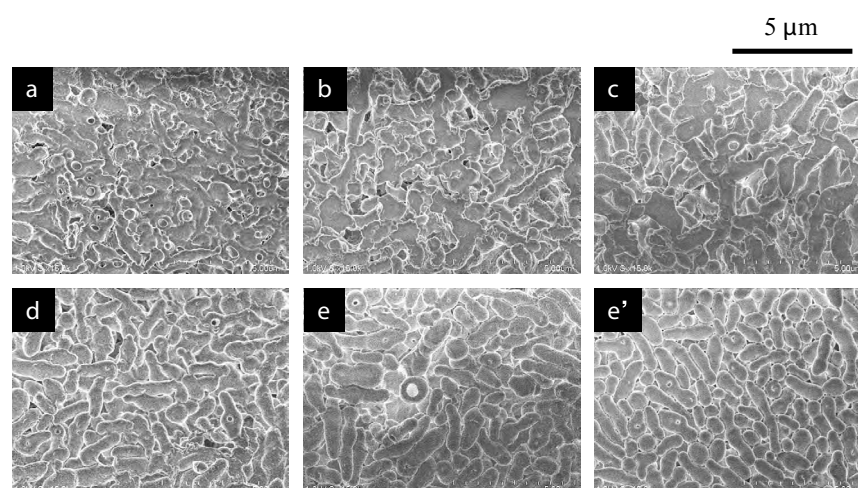


FIG. 5. The light scattering intensity, hydrodynamic size (Dh), and transmittance of the worm-like vesicles versus the temperature. The vesicle concentration=6.75 g/L.



**FIG. 6. The SEM images of the worm-like vesicles for the temperature increase: a 25°C, b 30°C, c 35°C, d 40°C, e 45°C, and f 50°C. The vesicle concentration = 6.75 g/L**



**FIG. 7. The SEM images of the worm-like vesicles for the temperature decrease: a 50°C, b 45°C, c 40°C, d 35°C, e 25°C, and e' 25°C and the ripening. The vesicle concentration=6.75 g/L.**

provided the anastomosed tubular networks and fenestrated sheets. It was found that spherical vesicles were reproduced by budding separation from the round swollen tubules composing the anastomosed tubular networks developed out of the fenestrated sheets by the expansion of the fenestrations. The worm-like vesicles were transformed into shorter and spherical vesicles and finally into fused aggregates by a temperature increase. By decreasing the temperature, worm-like vesicles were reproduced from the fused aggregate matrix through the transformation into partial sheets and further into anastomosed tubules, however, the resulting vesicles were round and short as compared with the original vesicles. The worm-like vesicles were more thermally stable than the spherical vesicles at the same vesicle concentration and retained the vesicular structure at high temperature. This is the first study demonstrating that the anastomosed tubular networks and fenestrated sheets are formed in the process of the thermal transformation of the vesicles and that the worm-like vesicles and spherical vesicles have different thermo stability. The study implies that this bio membrane model using the polymer giant vesicles has the potential to artificially create the morphological changes of lipid bilayer between and within organelles in living cells.

### Conflict of Interest

The author declares no conflict of interest in this study.

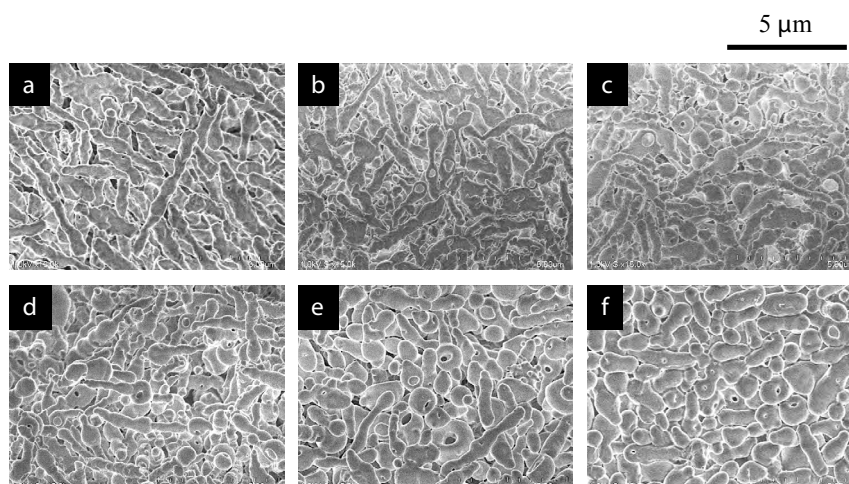


FIG. 8. The SEM images of the worm-like vesicles for the temperature increase at a high vesicle concentration: a 25°C, b 35°C, c 40°C, d 45°C, e 50°C, f 25°C after decreasing the temperature. The vesicle concentration=27.0 g/L.

### Acknowledgment

The author is thankful for a JSPS Grant-in-Aid for Scientific Research (Grant Number 25390003).

### REFERENCES

1. Diaz R, Mayorga LS, Weidman PJ, et al. Vesicle fusion following receptor-mediated endocytosis requires a protein active in Golgi transport. *Nature*. 1989;339(6223):398-400.
2. Conner SD, Schmid SL. Regulated portals of entry into the cell. *Nature*. 2003;422(6927):37-44.
3. Pelletier L, Jokitalo E, Warren G. The effect of Golgi depletion on exocytic transport. *Nat Cell Biol*. 2000;2(11):840-6.
4. Kang B, Staehelin LA. ER-to-golgi transport by COPII vesicles in Arabidopsis involves a ribosome-excluding scaffold that is transferred with the vesicles to the Golgi matrix. *Protoplasma*. 2008;234(1-4):51-64.
5. Orci L, Stannnes M, Ravazzola M, et al. Bidirectional transport by distinct populations of COPI-coated vesicles. *Cell*. 1997;90(2):335-49.
6. Rabouille C, Klumperman J. The maturing role of COPI vesicles in intra-Golgi transport. *Nat Rev Mol Cell Biol*. 2005;6(10):812-8.
7. Tolley N, Sparkes I, Craddock CP, et al. Trans membrane domain length is responsible for the ability of a plant reticulon to shape endoplasmic reticulum tubules in vivo. *Plant J*. 2010;64(3):411-8.
8. Kasuga S, Harada Y. Three-dimensional observation of the Golgi apparatus in Rat tracheal gland during the secretory cycle. *Auris Nasus Larynx*. 1990;17(4):243-8.
9. Koga D, Ushiki T. Three-dimensional ultrastructure of the Golgi apparatus in different cells: High-resolution scanning electron microscopy of osmium-macerated tissues. *Arch Histol Cytol*. 2006;69(5):357-74.
10. Tanaka K, Mitsushima A, Fukudome H, et al. Three dimensional architecture of the Golgi complex observed by high resolution scanning electron microscopy. *J Submicrosc Cytol*. 1986;18(1):1-9.

11. Guizzunti G, Seemann J. Mitotic Golgi disassembly is required for bipolar spindle formation and mitotic progression. PNAS. 2016;113(43):E6590-9.
12. Oke BO, Suarez-Quian CA. Partitioning of the Golgi apparatus in rat primary and secondary spermatocytes during meiosis. Anat Rec. 1992;233(2):245-56.
13. Zeng W, Locke M. The persistence of Golgi complexes during cell division in an insect epidermis. Tissue Cell. 1993;25(5):709-23.
14. Lucocq JM, Warren G. Fragmentation and partitioning of the Golgi apparatus during mitosis in HeLa cells. EMBO J. 1987;6(11):3239-46.
15. Yoshida E. Giant vesicles prepared by nitroxide-mediated photo-controlled/living radical polymerization-induced self-assembly. Colloid Polym Sci. 2013;291(11):2733-9.
16. Yoshida E. Morphological changes in polymer giant vesicles by intercalation of a segment copolymer as a sterol model in plasma membrane. Colloid Polym Sci. 2015;293(6):1835-40.
17. Yoshida E. Crosslinking effect of hydrophobic cores on morphology of giant vesicles formed by amphiphilic random block copolymers. Colloid Polym Sci. 2015;293(4):1275-80.
18. Yoshida E. Enhanced permeability of Rhodamine B into bilayers comprised of amphiphilic random block copolymers by incorporation of ionic segments in the hydrophobic chains. Colloid Polym Sci. 2015;293(8):2437-43.
19. Israelachvili JN. Intermolecular and Surface Forces, 3rd Edition. Waltham: Academic Press; 2011. 535 p.
20. Yoshida E. Morphology transformation of micrometer-sized giant vesicles based on physical conditions for photopolymerization-induced self-assembly. Supramol Chem. 2015;27(4):274-80.
21. Yoshida E. Worm-like vesicle formation by photo-controlled/living radical polymerization-induced self-assembly of amphiphilic poly(methacrylic acid)-block-poly(methyl methacrylate-random-methacrylic acid). Colloid Polym Sci. 2016;294(11):1857-63.
22. Yoshida E. Fabrication of microvillus-like structure by photopolymerization-induced self-assembly of an amphiphilic random block copolymer. Colloid Polym Sci. 2015;293(6):1841-5.
23. Yoshida E. Morphology control of giant vesicles by composition of mixed amphiphilic random block copolymers of poly(methacrylic acid)-block-poly(methyl methacrylate-random-methacrylic acid). Colloid Polym Sci. 2015;293(1):249-56.
24. Yoshida E. Morphology control of giant vesicles by manipulating hydrophobic-hydrophilic balance of amphiphilic random block copolymers through polymerization-induced self-assembly. Colloid Polym Sci. 2014;292(3):763-9.
25. Yoshida E. Hydrophobic energy estimation for giant vesicle formation by amphiphilic poly(methacrylic acid)-block-poly(alkyl methacrylate-random-methacrylic acid) random block copolymers. Colloid Polym Sci. 2014;292(10):2555-61.
26. Yoshida E. Morphological changes in giant vesicles comprised of amphiphilic block copolymers by incorporation of ionic segments into the hydrophilic block chain. Cogent Chem. 2016;2(1):1212319/1-16.
27. Yoshida E. Giant vesicles comprised of mixed amphiphilic poly(methacrylic acid)-block-poly(methyl methacrylate-random-methacrylic acid) diblock copolymers. Colloid Polym Sci. 2015;293(11):3641-8.
28. Yoshida E. Fission of giant vesicles accompanied by hydrophobic chain growth through polymerization-induced self-

- assembly. *Colloid Polym Sci.* 2014;292(6):1463-8.
29. Yoshida E. PH response behavior of giant vesicles comprised of amphiphilic poly(methacrylic acid)-block-poly(methyl methacrylate-random-methacrylic acid). *Colloid Polym Sci.* 2015;293(2):649-53.
  30. Yoshida E. Nitroxide-mediated photo-controlled/living radical polymerization of methacrylic acid. *Open J Polym Chem.* 2013;3(1):16-22.
  31. Marquardt DW. An algorithm for least-squares estimation of nonlinear parameters. *J Soc Indust Appl Math.* 1963;11(2):431-41.
  32. Kobayashi S, Uyama H, Yamamoto I, et al. Preparation of monodispersed poly(methyl methacrylate) particle in the size of micron range. *Polym J.* 1990;22(8):759-61.